Self-Focusing During Femtosecond Micromachining of Silicate Glasses

Lawrence Shah, Jess Tawney, Martin Richardson, and Kathleen Richardson

***Abstract*—Many recent investigations of micromachining with lasers, in vacuum and in ambient air environments, have demonstrated the improvements possible when using femtosecond-duration laser pulses compared with long laser pulses. There are obvious practical advantages for rapid micromachining in ambient air conditions. However, the maximum laser intensity and repetition rate are then eventually limited by the avalanche breakdown and nonlinear effects in the air through which the focused laser beam must propagate both outside the work piece and within the structure that is being machined. This paper investigates these limits in femtosecond deep hole drilling at high laser intensities in silicate glasses. In particular, it shows how nonlinear optical effects, particularly self-focusing, can dramatically affect hole shape and the rate of penetration during deep hole drilling. The experiments described here demonstrate how nonlinear Kerr focusing of femtosecond laser pulses occurs during propagation of intense femtosecond laser pulses through the atmosphere within the machined channel at powers levels significantly below the critical power for self-focusing in ambient air.**

***Index Terms*—Ablation, glass, laser, micromachining, optical self-focusing, plasma properties, ultrafast optics.**

I. Introduction

It is known that femtosecond lasers have several advantages over conventional laser systems for materials processing applications. These include the reduction of collateral damage in dielectrics [1], smaller heat-affected zones (HAZ) [2], a deterministic [3] rather than statistically distributed ablation threshold [4]–[6], and the ability to ablate subdiffraction-limit target regions [7]–[10]. This has encouraged increasing interest in the use of femtosecond lasers for precise micro-structuring of a wide range of materials for applications in medicine, aerospace, microelectronics, photonics, and other industries. The range of applications includes the writing of three-dimensional (3-D) waveguides in bulk glasses [11]–[13] etching quasi-phase-matched (QPM) crystals to improve nonlinear properties [9], processing fiber composites [14], polymer-processing [15], [16] micro-structuring of silica aerogels [17], ablation of biological tissue [18]–[20], and the machining of high explosives [20].

For most applications, it is desirable to perform processing at atmospheric pressures in order to minimize production costs and time. However, for 100-fs laser pulses at the 1-mJ level, processing in air can lead to complications for focused spot sizes of <100 μm in diameter as the instantaneous laser power can be greater than 10^{10} W and the intensity can exceed 10^{14} W/cm^2. At such powers, the nonlinear index of refraction of air affects beam propagation and ionization of the ambient atmosphere must be considered.

In this paper, we describe how the penetration depth and rate of ablation of femtosecond laser pulses in silicate glasses at atmospheric pressure are affected by drilling parameters such as laser intensity, target material, and repetition rate. We demonstrate that femtosecond laser pulses are capable of drilling deep holes (>1 mm depth) with high aspect ratios ($>10:1$)[21]. Most interestingly, our results show that there is a critical depth, which depends on the laser intensity and the composition of the target material, beyond which the process of self-focusing limits the effectiveness of deep hole drilling.

II. Ablation Mechanics

To understand the differences between ultrashort- (femtosecond) and long- (nanosecond) pulse laser ablation, it is necessary to review the fundamental differences in laser material interactions on these time scales. These differences are most evident during the ablation of transparent media. Since linear absorption is negligible, the transfer of energy from the laser beam to the target material is predominantly a laser plasma process where the laser plasma is formed by the two-step process of seeded avalanche ionization. For picosecond or longer laser pulses, free-electron seeds are generated by the ionization of surface carriers (typically defects or impurities) [4]–[6]. Due to the nonuniform distribution of surface carriers in transparent media, no precisely defined optical damage threshold exists so long as the ionization bandgap of the material is greater than the energy/photon [4]–[6], [22]. By contrast, ultrashort laser pulses (<1 ps) with intensities in excess of $\sim 10^{12}$ W/cm^2 are capable producing seeds by freeing bound electrons via multi-photon ionization (MPI) [1], [3], eliminating the reliance on surface carriers, resulting in a deterministic optical damage threshold [3]. In a process known as inverse Bremsstrahlung absorption, or joule heating, the seed electrons described above oscillate in the electric field of the laser pulse and absorb laser energy through dephasing collisions with bound electrons [3], [4],

Manuscript received October 3, 2002; revised August 18, 2003. This work was supported by the State of Florida.

L. Shah is with the Laser Plasma Laboratory, School of Optics & CREOL, University of Central Florida, Orlando, FL 32816 USA. He is also with the IMRA America, Inc., Ann Arbor, MI 48105 USA.

J. Tawney is with the Laser Plasma Laboratory, School of Optics & CREOL, University of Central Florida, Orlando, FL 32816 USA and also with the The Charles Stark Draper Laboratory, Inc., Cambridge, MA 02139 USA.

M. Richardson is with the Laser Plasma Laboratory, School of Optics & CREOL, University of Central Florida, Orlando, FL 32816 USA.

K. Richardson is with the Glass Processing and Characterization Laboratory, School of Optics & CREOL, University of Central Florida, Orlando, FL 32816 USA.

Digital Object Identifier 10.1109/JQE.2003.821486

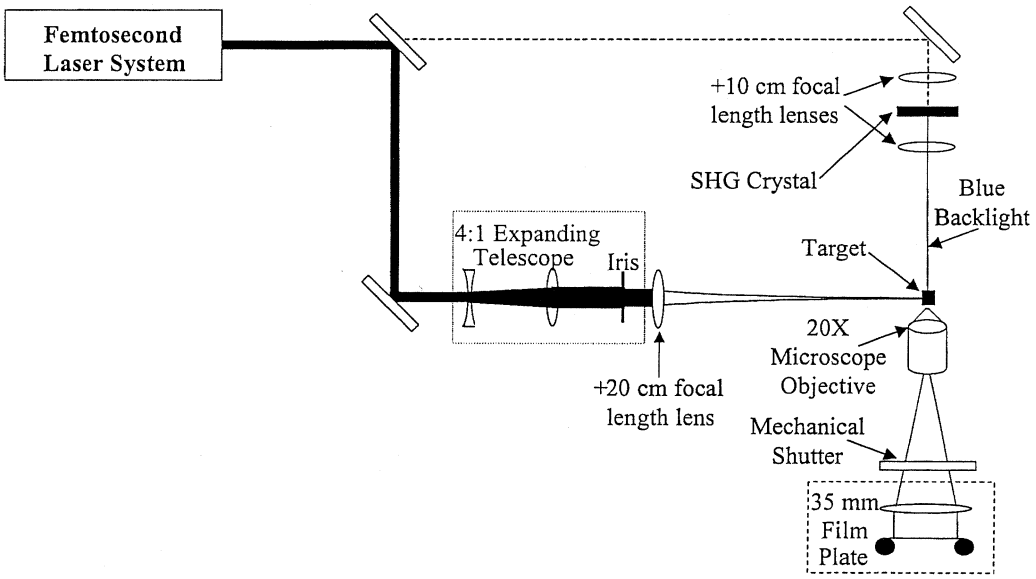

Fig. 1. Experimental setup.

[23]. Sufficiently energetic dephasing collisions cause the ionization of additional electrons, resulting in a chain reaction or "avalanche," producing a dense laser plasma.

For laser pulses longer than several picoseconds, energy is transferred from the laser pulse to the lattice by carrier-phonon coupling while the laser illuminates the target. Carrier-phonon coupling, with typical relaxation times from hundreds of femtoseconds to picoseconds, provides sufficient time for laser-induced damage to occur via thermal mechanisms, such as melting, boiling, and/or phase explosion (also known as explosive boiling [24], [25]), depending upon the degree of heating. Conversely, there is insufficient time for lattice heating by carrier-phonon collisions during the incidence of a femtosecond laser pulse. In this case, the absorption of laser energy causes the rapid generation of a dense electron plasma via carrier–carrier collisions while the lattice remains at room temperature. After the impact of the laser pulse, energy is conducted from the electron plasma to the lattice by carrier-phonon coupling. Thus, the transition from long-pulse laser ablation to ultrashort-pulse laser ablation can be defined in terms of the carrier-phonon coupling relaxation time of the target material [26]–[28].

Due to the time lag between laser absorption and bulk material heating, ultrashort laser irradiation typically causes a highly nonequilibrium plasma temperature distribution. During high-fluence (<10 J/cm^2) femtosecond laser processing, the ablation process is essentially a phase explosion in which the target region is superheated, resulting in a direct solid-to-gas phase transition. Although we are not currently aware of any experiments to quantitatively characterize the size and/or temporal evolution of the ablated particles, the research of Sokolowshi-Tinten *et al.* and Cavalleri *et al.* demonstrates that, during femtosecond laser irradiation of semiconductors and metals, ablated material forms a smooth layer of expanding vaporized material [29]–[32]. These studies reveal that, although this vaporized material remains at nearly solid density for some time after being ejected from the target, the layer is transparent, indicating the absence of large particles (>1 μm) that would scatter or absorb the probe light ($\sim$750 nm).

III. Femtosecond Laser Drilling Above and Below the Air-Ionization Threshold

Most femtosecond laser machining experiments so far have been conducted at peak laser intensities below the air-ionization threshold ($\sim 10^{14}$ W/cm^2) or under vacuum conditions [8], [9], [11], [13], [28]–[35]. There would seem to be little reason for exceeding this intensity, since air ionization can rob energy from the laser pulse and/or distort the beam in space and time prior to the interaction with the target. In the present investigation, we set out to characterize the influence of the ambient air on the mechanics of femtosecond laser ablation as a function of the number of laser pulses incident during drilling of transparent glasses at intensities that are above and below the threshold for air ionization. In order to gauge the influence of the ionization bandgap on ablation, experiments were conducted using soda-lime silicate glass and 45% mol. PbO silicate glass (the ionization bandgap is $\sim$5 eV for soda-lime silicate glass and $\sim$2.5 eV for 45% mol. PbO silicate glass [36]).

The laser system used for these experiments consisted of a mode-locked Ti:sapphire oscillator and a flashlamp-pumped Cr:LiSAF regenerative amplifier, producing 110-fs [full-width at half-maximum (FWHM)] laser pulses with a maximum energy/pulse of 1.6 mJ at 845 nm and a repetition rate of 5 Hz [21]. The pulse-to-pulse variance of the laser energy was $\sim$10%. Prior to focusing by a convex/plano 20-cm-focal-length fused silica lens, the beam was expanded using a 4:1 telescope (Fig. 1). The focal beam waist was determined by measuring the beam profile with a knife-edge at three points beyond the focus of the lens and solving the appropriate Gaussian beam propagation equations. In earlier experiments comparing femtosecond and nanosecond laser machining of silicate glass [21], an iris was placed prior to the focusing lens was used to adjust its effective numerical aperture to the wavelength and

beam divergence of the three different lasers so as to produce a 100-μm (FW1/e^{2}M) beam diameter on focus. With this setup, no air ionization was observed at the maximum energy that could be delivered to target at 110-fs, 1.5-mJ/pulse (intensity, $I_p = 1.74 \times 10^{14}$ W/cm^2; fluence, $F_p = 19.1$ J/cm^2) [21]. Since it was not possible to increase the output power of the laser, the laser intensity on target was increased by removing the constricting iris (Fig. 1). The larger beam waist at the focusing lens reduced the focal spot size on the target to 75 μm (FW1/e^{2}M) from 100 μm (FW1/e^{2}M). Due to the change in focusing conditions, the M^2 value of the laser beam increased to $\sim$1.55 and the Rayleigh range ($Z_R = \pi w_o^2/\lambda$, where λ is the laser wavelength, and w_o is the laser focal radius) decreased to 5.2 mm (compared to $M^2 = 1.50$ and $Z_R = 9.5$ mm, for $d = 100$ μm). To compensate for the reduced focal diameter, the laser output power was reduced slightly so that the incident laser energy on target remained 1.5-mJ/pulse. As such, the laser intensity increased to 3.08×10^{14} W/cm^2 from 1.74×10^{14} W/cm^2 and the fluence increased to 33.9 J/cm^2 from 19.1 J/cm^2. At this intensity, ionization of the air at the focal spot (no target) produced a visible and audible plasma spark. Drilling experiments were conducted with the target surfaces of the two types of glasses in contact with the air spark. Since the air-ionization experiments were performed virtually at the air ionization threshold, the center of the air spark was used to indicate the location of the focal plane to within a precision of $\sim$100 μm.

Hole-drilling experiments were conducted with the focus and the glass target position fixed while a set number of laser pulses impacted each sample. The incident beam was linearly polarized, with the polarization axis parallel to the plane of the image in the figures. Optical micrographs taken after laser processing revealed that the relatively small difference in the incident femtosecond laser intensity resulted in a significant change in the holes produced. Holes produced by the impact of 10^4 laser pulses, in soda-lime silicate glass and in 45% mol. PbO silicate glass, are shown in Fig. 2. These results have been previously reported in greater detail [21]. The holes are similar in shape, in that they are smooth, with no sign of collateral damage to the surrounding material, and the entrance diameter is only slightly larger than the measured FW1/e^{2}M of the beam. Thus, it is possible to machine silicate glasses precisely, with negligible HAZ at intensities both above and below the threshold for air ionization. However, it is clear that the increase in laser intensity causes significant changes in the maximum laser penetration depth and leads to bending of the machined hole deep inside the bulk material for both silicate glass and PbO silicate glass.

It is at first difficult to understand how this modest increase in laser intensity causes the maximum penetration depth to *decrease* in soda-lime silicate glass, but to *increase* in lead silicate glass. A plot of the penetration depth of the laser versus the number of incident pulses helps to provide some insight. Fig. 3 shows that, in the lower intensity case, the penetration rate is constant throughout the experimental range for both glasses at $\sim$0.20 μm/pulse (solid lines). However, during drilling at the higher laser intensity, there is a dramatic change in the penetration rate (dotted lines). In both glasses, the penetration

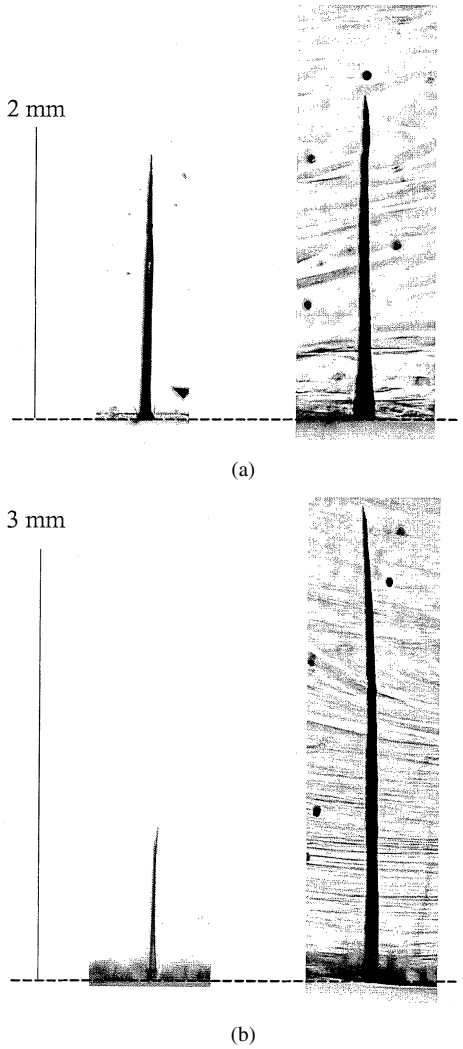

Fig. 2. Profile of femtosecond laser machined holes after 10^4 pulses in soda-lime silicate glass (left) and 45% mol. PbO silicate glass (right) for: (a) $I_p = 1.74 \times 10^{14}$W/cm^2, $d = 100$ μm (FW1/e^{2}M) and (b) $I_p = 3.08 \times 10^{14}$ W/cm^2, $d = 75$ μm (FW1/e^{2}M).

rate initially starts at a very high value ($\sim$0.50 μm/pulse) but then, quite abruptly, decreases by an order of magnitude to $\sim$0.05 μm/pulse. The point at which rollover occurs is different in the two glasses, occurring after $\sim$5000 pulses in lead silicate and after $\sim$1000 pulses in soda lime silicate; however, the initial and final penetration rates are independent of the target material.

IV. Optical Probe Results

In order to gain a better understanding of the mechanics of material removal as a function of the number of laser pulses during ablation above the air-ionization threshold, we simultaneously captured profile images of the hole and images of the laser produced plasma using a time-shuttered film plate (Fig. 1). A small portion of the laser pulse ($\sim$0.1%) was converted to $\lambda = 422$ nm using a KD*P frequency-doubling crystal, providing a synchronized visible illumination source. This blue light was used to backlight the hole, allowing us to obtain optical micrographs of the depth versus the number of laser pulses during the drilling of a single hole. Photos were taken with a

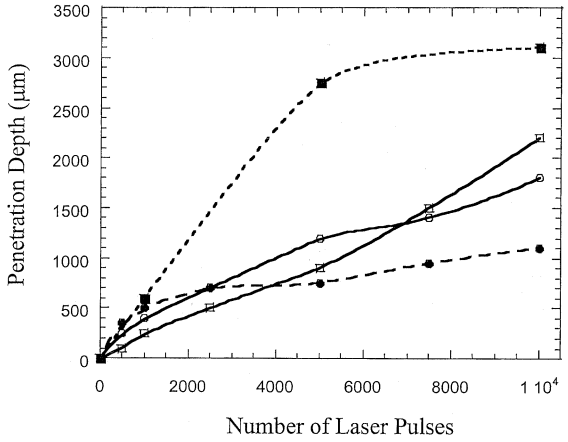

Fig. 3. Femtosecond laser penetration depth as a function of number of incident laser pulses in soda-lime (circles) and in 45% mol. PbO silicate (squares) glasses, for: $I_p = 1.74 \times 10^{14}$ W/cm^2, $d = 100$ μm (FW1/e^{2}M) (solid lines) and $I_p = 3.08 \times 10^{14}$ W/cm^2, $d = 75$ μm (FW1/e^{2}M) (dotted lines).

shutter speed of 1/125 s, collecting both the blue backlight and the visible emission of the laser-induced plasma spark. The images permitted the observation of the plasma spark and the shape of laser drilled hole relative to depth.

With the shutter speed of the film stop set at 1/125 s, each photo corresponds to the impact of a single pulse from the 5-Hz laser system. Figs. 4 and 5 are "movies" showing the results of two such experiments, performed at different laser intensities in soda-lime silicate glass, where each frame is separated by 30 s, $\sim$150 laser pulses. In this set of experiments, the beam focal diameter was 75 μm (FW1/e^{2}M), with: $E_p = 1.5$ mJ/pulse and $I_p = 3.08 \times 10^{14}$ W/cm^2 (Fig. 4) and $E_p = 1.0$ mJ/pulse and $I_p = 2.06 \times 10^{14}$ W/cm^2 (Fig. 5). Given the relatively small focal spot, the laser intensity was sufficient at both intensities to produce a plasma spark in air when no target was present. These movies demonstrate that there is a clear change in the uniformity of the laser-produced plasma in the channel as the number of laser pulses increases.

A graph of the femtosecond laser penetration rate in soda-lime silicate glass, plotted from the data obtained from time-lapse photographs of drilling runs at the two laser intensities (Fig. 6), further illustrates the rollover in the ablation rate observed in Fig. 3 during drilling above the air ionization threshold. Despite the identical focal beam diameter and the associated Rayleigh range in Figs. 4–6, the less intense femtosecond laser pulses penetrated *more* deeply into the sample. At the higher powers in Fig. 6 the penetration rate rapidly reduces from the initial rate of 0.50 μm/pulse to a near flat-line value of $\sim$0.05 μm/pulse. The case is similar for $E_p = 1.0$ mJ/pulse and $I_p = 2.06 \times 10^{14}$ W/cm^2, however the rollover is more gradual and occurs later allowing the femtosecond laser pulses at this lower intensity to penetrate more deeply into the sample. Fig. 6 also shows that the rollover in penetration depth is repeatable, suggesting that the point of the rollover is intensity dependent. The repeatability of this data suggests that the change in the ablation mechanism is not sensitive to experimental instabilities. The initial penetration rate was $\sim$0.5 μm/pulse for both intensities. However in the lower intensity case, the penetration rate reduced slightly at $\sim$1000 pulses to a rate of $\sim$0.40 μm/pulse, then flattened out after $\sim$3000 pulses; whereas there was a single sudden drop in penetration rate at $\sim$1200 pulses for the higher intensity case.

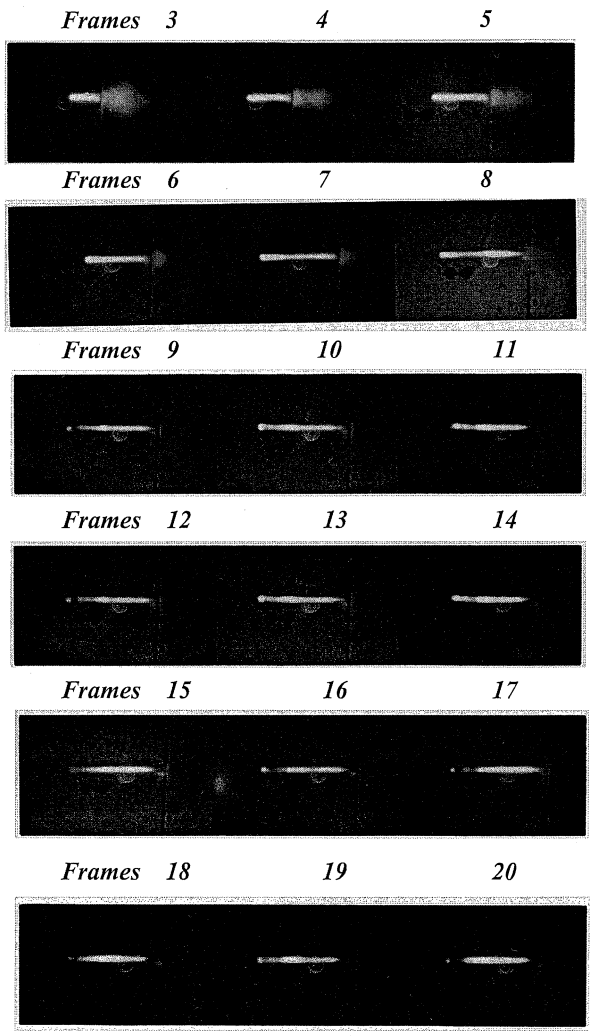

Fig. 4. Time-lapse images (one frame every 30 s, corresponding to the impact of 150 laser pulses) of drilling of soda-lime silicate glass, for: $E_p = 1.5$ mJ, $I_p = 3.08 \times 10^{14}$ W/cm^2, $d = 75$ μm, and$t_p = 110$ fs.

A closer look at the *in-situ* photographic data illustrates the change in the laser-produced plasma distribution before and after the rollover points indicated by Fig. 6 and provides clues about the mechanism causing the change in processing conditions. In frames 3–6 of Fig. 4 and in frames 2–10 of Fig. 5, the plasma fills the channel uniformly. The larger images in Fig. 7 show almost no sign of hole tapering at this stage. As such, the diameter of the hole and the ablation rate remain nearly constant, indicating that each laser pulse ablates a disk of material $\sim$50 μm in diameter and $\sim$0.50 μm thick (ablated volume is $\sim 10^{-9}$ cm^3). The situation changes in frames 7–10 of Fig. 4 and in frames 11–14 of Fig. 5. At this point, the laser plasma no longer uniformly fills the hole, and the ablating tip is much narrower. Furthermore, these frames clearly demonstrate that the plasma cools before it can completely escape from the hole, therefore it is likely that a significant amount of the ablated material remains trapped inside the channel until the impact of the

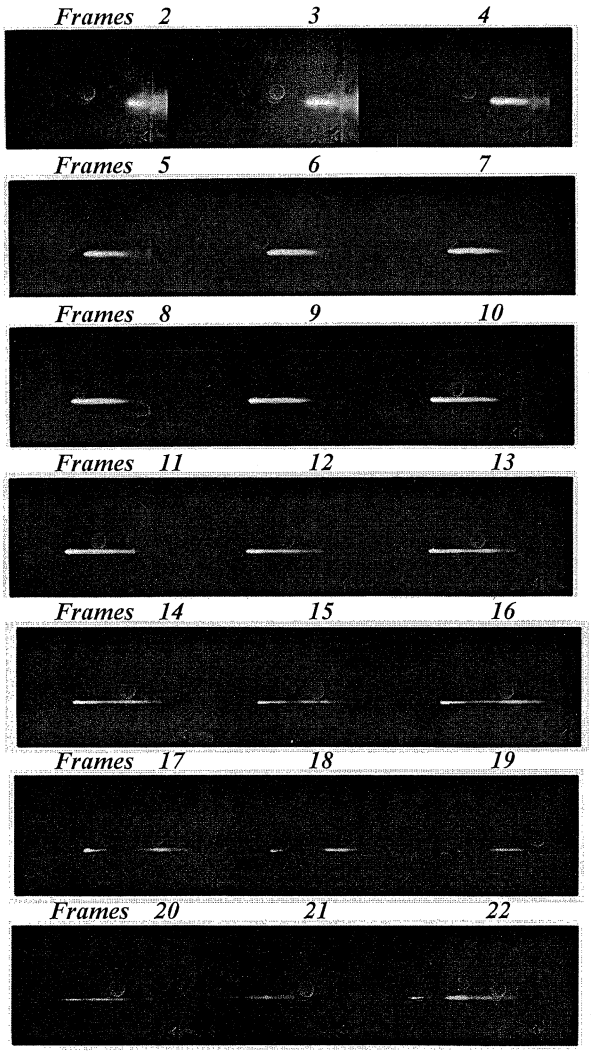

Fig. 5. Time-lapse images (one frame every 30 s, corresponding to the impact of 150 laser pulses) of drilling of soda-lime silicate glass, for: $E_p = 1.0$ mJ, $I_p = 2.06 \times 10^{14}$ W/cm^2, $d = 75$ μm, and$t_p = 110$ fs.

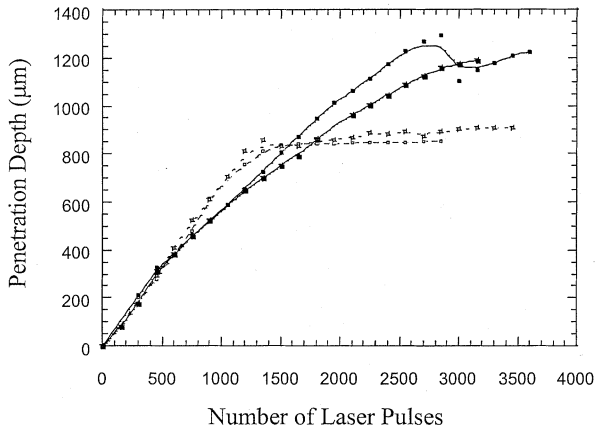

Fig. 6. Femtosecond laser penetration depth in soda-lime silicate glass vs. the number laser pulses, for: $E_p = 1.0$ mJ/pulse, $I_p = 2.06 \times 10^{14}$ W/cm^2, $F_p = 22.4$ J/cm^2, $d = 75$ μm (solid lines) and $E_p = 1.5$ mJ/pulse, $I_p = 3.08 \times 10^{14}$ W/cm^2, $F_p = 33.9$ J/cm^2, $d = 75$ μm (dotted lines).

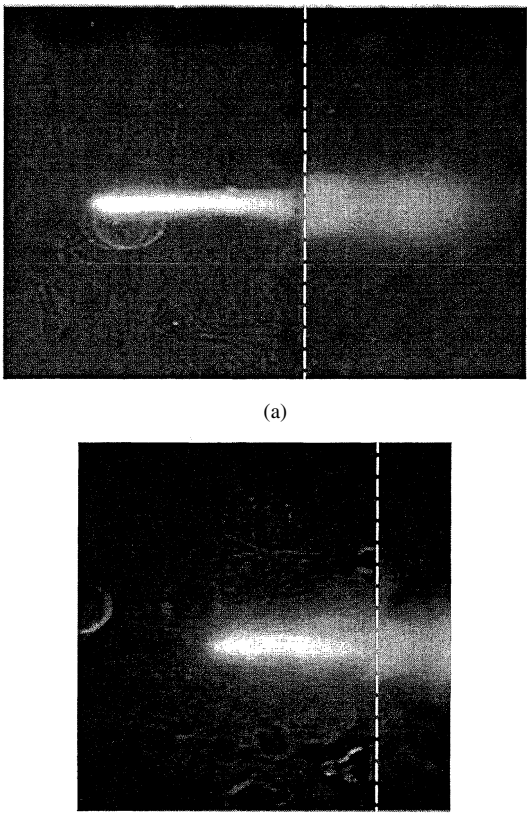

(a)

(b)

Fig. 7. Enlargements of (a) frame 4 from Fig. 4 and (b) frame 3 from Fig. 5 showing the early stages of the hole development. The laser propagated from right to left, and the target surface is indicated by the dotted line.

subsequent laser pulse despite the relatively long time between pulses (~200 ms). Finally, by frame 17 in Figs. 4 and 5, the plasma has broken into two main sections consisting of a bright area about half way down the hole and a smaller bright spot at the deepest part of the hole. Although the laser-produced plasma is brightest in the middle of the hole, subsequent photos indicate that there is no appreciable widening of the laser channel associated with this area. Rather, ablation is restricted to the deep end of the hole where the tip of the plasma is in contact with the bulk material.

Thus, we have broken the evolution of femtosecond-laser-pulse deep drilling of soda-lime silicate glass into three phases. Initially, the laser plasma is a uniform cylinder of ~50 μm in diameter, filling the channel to a maximum depth of ~500 μm. At this stage, a portion of the laser-produced plasma is visible escaping from the hole (Fig. 7). During the transition phase associated with the intensity-dependent rollover points, the plasma distribution becomes nonuniform and no luminous plasma can be seen escaping from the hole (Fig. 8). In the final stage, there is a dramatic reduction in ablation rate (Fig. 6) and ablation is associated with a small plasma tip at the deepest point of the laser machined hole (Figs. 9–11).

Since the rollover in ablation rate is more gradual for $E_p = 1.0$ mJ/pulse and $I_p = 2.06 \times 10^{14}$ W/cm^2 than in the highest intensity case (Fig. 6), Fig. 5 provides a great deal of information about changes in the ablation mechanics. Frames 14–17 show a gradual transition from the initial stage, in which the plasma is uniform, to the final stage, where the plasma breaks apart. In particular, these frames show that a narrow plasma filament,

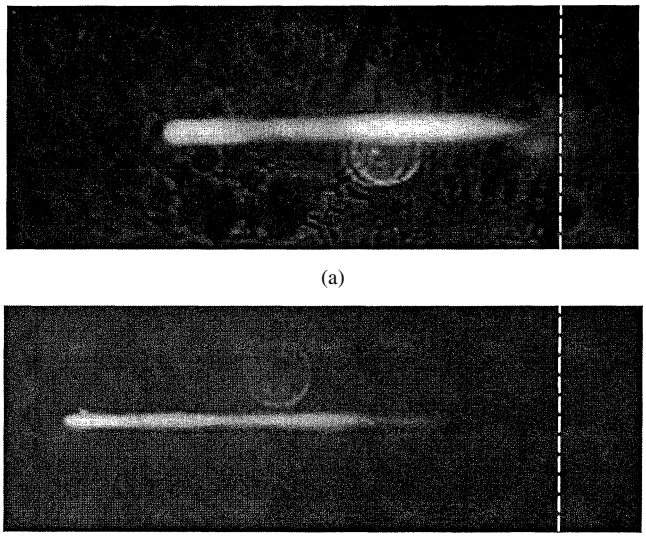

(a)

(b)

Fig. 8. Enlargements of (a) frame 8 from Fig. 4 and (b) frame 13 from Fig. 5 demonstrating changes in the laser produced plasma profile. The laser propagated from right to left, and the target surface is indicated by the dotted line.

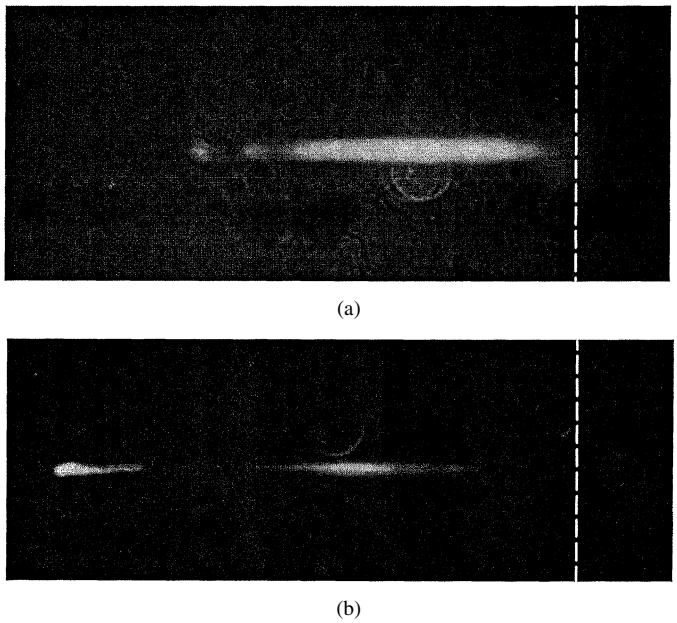

(a)

(b)

Fig. 9. Enlargement of (a) frame 17 from Fig. 4 and (b) frame 17 from Fig. 5 showing the final stage in the evolution of the laser produced plasma. The laser propagated from right to left, and the target surface is indicated by the dotted line.

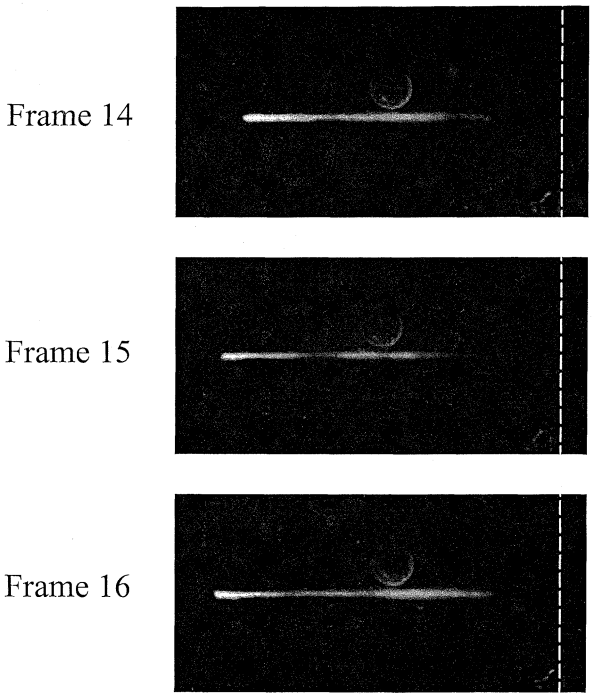

Fig. 10. Enlargements of frames 14–16 of Fig. 5 illustrating the separation of the plasma into two pieces connected by a narrow ($\sim$10 μm in diameter) filament. The laser propagated from right to left, and the target surface is indicated by the dotted line

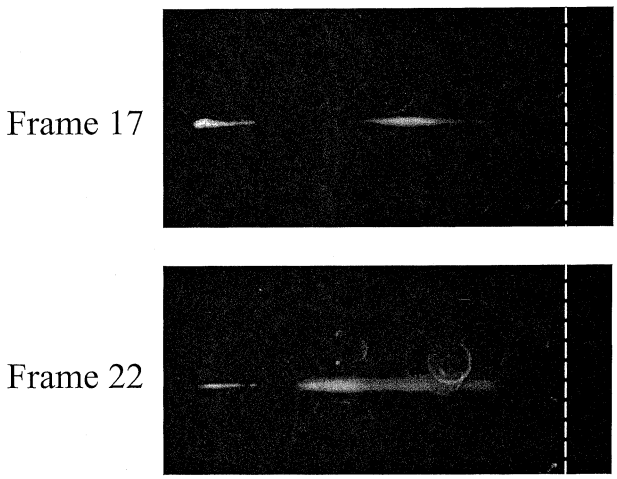

Fig. 11. Enlargements of frames 17 and 22 from Fig. 5 showing the wander of the ablating plasma tip. The laser propagated from right to left, and the target surface is indicated by the dotted line.

$\sim$10 μm in diameter, connects the regions of plasma as they begin to separate and forms a tip associated with ablation at the hole bottom (Fig. 11). Fig. 11 also demonstrates that the ablating plasma tip moves from pulse to pulse. In frame 17, the plasma tip is ablating material toward the lower portion of the hole while the plasma filament bends slightly deep inside the hole. However, by frame 22 the plasma filaments have straightened out and ablate material from the region slightly above the region ablated in frame 17. The jitter associated with the plasma filament deep inside the channel helps to explain the rollover in Figs. 3 and 6, in that although each shot ablates additional material there is negligible increase in the depth of the hole because each pulse hits a different spot. Finally, the process of plasma filamentation also helps to explain the bending of the holes machined in soda-lime and PbO silicate glasses [Fig. 2(b)].

It is important to note here that there is no evidence of air ionization significantly disturbing the beam propagation until a critical depth is reached. Figs. 3 and 6 show that femtosecond laser ablation above the air-ionization threshold initially leads to larger penetration rates, and Figs. 4 and 5 demonstrate that the beam could penetrate over 500 μm without a reduction in ablation rate. Although the independence of the initial rate of ablation on the incident laser fluence/intensity, shown in Fig. 6, suggests that the ablation rate has been saturated. Figs. 4–6 illus-

trate that the situation is dramatically different in soda-lime silicate after ~1000 laser pulses. Figs. 4–11 show that the plasma became nonuniform at a depth of 800–1200 μm, corresponding to the rollover points in Figs. 3 and 6. It is not until the rollover point, determined by the target material (Fig. 3) and incident laser intensity (Fig. 6), that laser interaction with the air in the channel appears to significantly reduce the ablation rate. It is unlikely that the hole geometry is the determining factor is this process, since the diameter and taper of the holes does not vary greatly between soda-lime and PbO silicate glasses (Fig. 2). Rather, the intensity and material dependence of self-focusing suggests that it is the result of the nonlinear phenomenon inside the channel.

We believe the change in ablation characteristics shown in Figs. 2–11 corresponds to unstable beam steering induced by self-focusing of the femtosecond laser during its propagation down the hole. The fact that the onset of self-focusing is different for the silicate glasses studied here (Fig. 3) does not appear to be a consequence of laser-induced ionization of the ambient atmosphere. Furthermore, the maximum penetration depth in soda-lime silicate glass appears to be dependent upon laser fluence/intensity (Fig. 6) rather than the Rayleigh range. We also believe the cumulative effect of self-focusing, over hundreds and thousands of shots, is responsible for the bends observed in the holes produced using 10^4 laser pulses in Fig. 2(b). Although these results leave several questions unanswered, such as the influence of laser polarization and the shape of the hole in the plane perpendicular to the images in Figs. 2, 4, 5, and 7–13, they suggest that beam pointing changes more or less randomly from pulse to pulse as a result of beam filamentation while drilling deep holes above the threshold for air ionization. Thus, the shape of the hole beyond a depth of ~800 μm represents the statistical summation of the more-or-less random beam deflection associated with the aiming stability of the plasma filament.

V. Nonlinear Interactions With the Atmosphere

A. Kerr Lensing

It is well known that nonlinear self-focusing is initiated by the positive lens created by the intensity-dependent modification of the index of refraction induced by an intense Gaussian laser beam profile via the Kerr effect. The intensity-dependent index of refraction is defined as [37]

$$n = n_0 + n_2 I \tag{1}$$

where the nonlinear index of refraction is given by

$$n_2(\text{esu}) = \frac{12\pi^2}{n_0^2 c}\chi^{(3)}(\text{esu}) \tag{2}$$

$$n_2\left(\frac{cm^2}{W}\right) \cong n_2(\text{esu}) x 10^3. \tag{3}$$

Above a certain critical power, the positive Kerr lens is sufficient to overcome diffraction and will produce a "new" beam waist at a distance z_f from the original focus point [37]

$$z_f = \frac{2n_0}{0.61}\frac{w_0^2}{\lambda}\frac{1}{(P/P_{\text{cr}})^{1/2}} \tag{4}$$

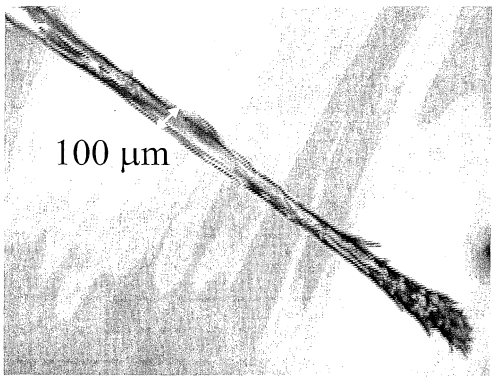

Fig. 12. Micrograph of hole drilled into 45% PbO glass after 10^5 laser pulses (100 exposures of 1 s each), for $t_p = 150$ fs, $\lambda = 775$ nm, $I_p = 1.25 \times 10^{14}$W/cm^2, and $R = 1$ kHz.

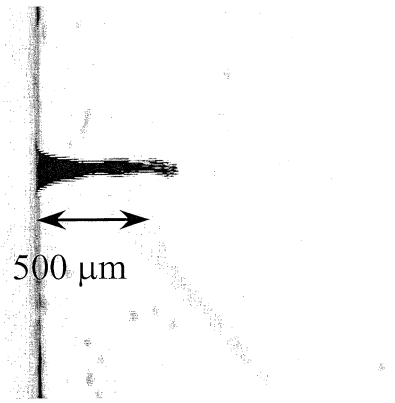

Fig. 13. Optical micrograph of a hole drilled into soda-lime silicate glass after 3200 laser pulses (400 exposure of 0.008 seconds each), for $t_p = 150$ fs, $\lambda = 775$ nm, $I_p = 1.25 \times 10^{14}$ W/cm^2, and $R = 1$ kHz.

where the critical power for this self-focusing is [37]

$$P_{\text{cr}} = \frac{\pi(0.61\lambda)^2}{8n_0 n_2}. \tag{5}$$

Thus, it is necessary to know the value of the nonlinear index of refraction n_2 or the third-order susceptibility $\chi^{(3)}$ in order to determine the strength of nonlinear self-focusing.

Table I provides the published values for n_2 and/or$\chi^{(3)}$ and the corresponding values calculated using (2) and (3) (taking into account the different units used). It shows that the published values for n_2 range through a full order of magnitude from 5.6×10^{-19} [38] to 5.9×10^{-20} cm^2/W [39], depending upon the specifics of the experimental technique and/or the theoretical assumptions made.

Experiments on the propagation of femtosecond laser pulses in air have demonstrated that diffraction is balanced by self-focusing at a critical power of $P_{\text{cr}} \sim 10$ GW for a 200-fs laser pulse with a center wavelength of 775 nm [43], which implies that n_2 is $\sim 1 \times 10^{-19}$ cm^2/W. Using this value for the critical power of self-focusing in (4), the minimum self-focusing length given the experimental conditions described in Sections III and IV ($w_0 = 37.5\,\mu$m, $\lambda = 845$ nm, and $P = 1.5 \times 10^{10}$ W) would be ~4.5 mm. Even if n_2 were taken to be 5.6×10^{-19} cm^2/W, implying a critical power for self-focusing of 1.8 GW [38], the self-focusing length is ~1.9 mm. However, the optical probe

TABLE I
SELF-FOCUSING DATA IN AIR (*ORIGINAL VALUES)

Author	$\chi^{(3)}$ (cm^3/erg)	n_2 (esu)	n_2 (cm^2/W)	P_{cr} (W)
Boyd[37]	*1.2x10^{-17}		4.7x10^{-19}	2.2x10^9
Chiron[38]			*5.6x10^{-19}	1.8x10^9
Rado[39]	*~1.5x10^{-18}		5.9x10^{-20}	1.7x10^{10}
Vlasov[40]	*4.6x10^{-18}	*2.5x10^{-16}	1.8x10^{-19}	5.7x10^9
Shimoji[41]		*1.7x10^{-16}	1.2x10^{-19}	8.6x10^9
Martin[42]			*~2.5x10^{-19}	4.2x10^9

experiments shown in Fig. 4 demonstrate beam filamentation within 0.800 μm.

B. Plasma Defocusing

As the incident laser power increases, Kerr lensing results in ever tighter beam focusing. This effect is countered by plasma defocusing. A theoretical model of the nonlinear modification to the refractive index induced by strong electromagnetic waves was first proposed by Max *et al.* [44], based upon plasma dynamics. In this case, the incident laser field is linearly polarized, thus the electric field is

$$\vec{E} = \hat{x} E_0 \cos\chi_0 \tag{6}$$

where

$$\chi_0 = \omega_0 t - k_0 x \tag{7}$$

and the maximum incident electric field amplitude is E_0, the oscillation frequency is ω_0, and the wavenumber is k_0 [45].

For a sufficiently intense laser pulse, the instantaneous electric field can cause the formation of critically dense plasmas ($N_e \sim 1.3 \times 10^{21}$ cm^{-3} for $\lambda_0 = 850$ nm) within tens of femtoseconds [28] (see Section II). The interaction of ultrahigh-intensity laser beams with dense electron plasmas requires consideration of the influence of the plasma and the motion of the electrons in the plasma (in response to the Lorentz force and relativistic plasma dynamics) on the propagation in the incident laser pulse.

The Lorentz force associated with the electric and magnetic fields of the incident laser beam is given by

$$F = e(E + v_e \times B) \tag{8}$$

where E and B and the incident electromagnetic fields and v_e is the velocity of the electrons in the laser produced plasma [45]. In intense fields, free electrons will also acquire a relativistic Lorentz factor according to

$$\gamma_0 \cong 1 + \frac{1}{2}(\nu_0 \sin\chi_0)^2 \tag{9}$$

where the driving frequency χ_0 is given by (7) and ν_0 is the wave amplitude which results from the amplitude-dependent mass response of the electrons in the plasma to the incident laser field, given by [44]

$$\nu_0 \cong \frac{eE_0}{m_e c \omega_0} \tag{10}$$

where e is the electron charge, E_0 is the magnitude of the electric field, m_e is the electron mass, c is the speed of light in vacuum, and ω_0 is the laser frequency.

For modest laser intensities ($<10^{16}$ W/cm^2), the plasma-induced refractive index can be written in the form

$$\eta \approx 1 - \frac{1}{2}\frac{\omega_P^2}{\omega_0^2} + \frac{1}{8}\frac{\omega_P^2}{\omega_L^2} a_L^2 \tag{11}$$

where a_L is the amplitude of the normalized vector potential in terms of the peak incident electric field (here $a_L^2 \leq 1$, since relativistic electron motion is negligible [46]). ω_P is the plasma frequency shown as

$$\omega_P = \left(\frac{4\pi e^2 n_e}{m_e}\right)^{1/2} \tag{12}$$

where n_e is the electron density [46].

At the intensities examined in our research (10^{14} W/cm^2), the relativistic self-focusing [third term in (11)] is negligible. Thus, an electron plasma induces a reduction in refractive index which is proportional to the density of electrons in the plasma.

VI. DISCUSSION OF SELF-FOCUSING

Self-focusing of intense laser pulses occurs when the Kerr lens is sufficiently strong to overcome diffraction. If the laser intensity exceeds the ionization threshold, plasma defocusing will also affect beam propagation. Under some conditions, Kerr lensing will counteract diffraction and plasma defocusing, forming beam filaments which can propagate over several Rayleigh ranges. Such behavior has been observed in gases [43], [47]–[49] and solid transparent media [50]–[53]. Ultrashort pulse laser propagation is further complicated during hole drilling. Particularly during deep hole drilling, the ejection of ablated material is restricted by the geometry of the laser-machined channel. Any residual material remaining in the air within this channel will interact with subsequent laser pulses.

The results of Sections II and III indicate the existence of an intermediate regime (between solid and gas), in which the propagation medium is a suspension of ablated debris in air. Although it is not currently possible to do a constituent analysis or numerical simulation of the particles in the atmosphere of the laser drilled channel given our test conditions, it is likely that, as the depth to width ratio of the hole increases, a portion of the ablated material will remain suspended in the air during the time between laser pulses (0.2 s). The rate of material removal during deep hole drilling above the air ionization threshold reduced from $\sim 10^{-11}$ to $\sim 2.5 \times 10^{-13}$ cm^3/pulse, while the material removal rate was essentially constant at $10^{-11} - 10^{-12}$ cm^3/pulse (the penetration rate is ~ 0.2 μm/pulse, the hole diameter varies from 75 to 40 μm, the area of the hole is between 5 and 1×10^{-5} cm^{-3}) throughout the test range below the air breakdown threshold. We believe that this difference is the result

of laser interaction with the mixture of air and ablation residue similar to that observed by Klimentov *et al.* [54] and Ashkenasi *et al.* [55]. For example, Ashkenasi *et al.* reported that, during hole drilling in fused silica, the ablation rate remained essentially constant until a sudden saturation was reached [55]. This saturation depth was similar within a range of vacuum pressures from 10^{-4} to 1 mbar; but was much less at atmospheric pressure [55]. Klimentov *et al.* found that for laser pulses longer than several picoseconds atmospheric deep hole drilling was dominated by plasma screening effects; however, femtosecond deep hole drilling was strongly influenced by the nonlinear optical properties of the air/dust in the beam path [54]. For example, during deep hole drilling of steel in air with $\sim$100 fs laser pulses [54], no plasma screening was observed at fluences below 200 J/cm^2. However, 50%–60% of the incident beam was disturbed by nonlinear interactions for laser fluences from 30 to 60 J/cm^2. Beam disturbance was accompanied by conical emission [56] causing the formation of a shallow trench surrounding the main hole [54]. Some evidence of conical emission during our experiments can be seen surrounding the entrance holes in Fig. 2 (left images) and Fig. 13.

As described in Section IV, our results suggest a nonlinear interaction between the incident laser pulse and the air/dust in the machined channel, where the laser intensity is above the critical power for self-focusing but the laser fluence is below the threshold for the generation of dense electron plasma. This interaction passes through three stages as the hole penetrates into the material. In the first stage (before rollover), ablation occurs at a constant rate of $\sim$0.5 μm/pulse (assuming that the diameter of the hole is $\sim$50 μm, the area of the hole is $\sim 2 \times 10^{-5}$ cm^2, and the ablated volume is $\sim 10^{-11}$ cm^3/pulse), and the laser-produced plasma forms a uniform cylinder with a diameter of $\sim$50 μm. In the transition stage (during rollover), the rate of ablation reduces rapidly, the laser plasma brakes apart, and the hole taper increases. In the final stage (after rollover), laser plasma filamentation produces a wandering plasma tip ($\sim$10 μm in diameter) which penetrates at a constant rate of $\sim$0.05 μm/pulse (assuming that the diameter of the hole is $\sim$25 μm, the area of the hole is $\sim 5 \times 10^{-6}$ cm^2, and the ablated volume is $\sim 2.5 \times 10^{-13}$ cm^3 /pulse). Figs. 4–11 suggest that Kerr lensing and plasma defocusing compete with one another, causing beam filamentation when the hole reaches some critical depth which depends upon the target material (Fig. 3) and the incident laser intensity (Fig. 6).

Quantitative estimates of the absolute strength of the positive Kerr lens or the electron density in the channel are not possible; however, it is possible to make several qualitative statements about the mechanics of the self-focusing process. According to (5), the observed self-focusing length of $\sim$1 mm (Figs. 4 and 5) indicates that the critical power for self-focusing is less than 5×10^8 W and the nonlinear index of refraction is greater than 2×10^{-18} cm^2/W. Clearly, such a large value for the nonlinear refractive index of the atmosphere within the laser-machined channel cannot be explained simply in terms of typical values for the n_2 of air (Table I). Rather, the strength of the nonlinear lens suggests that the ablation residue has significantly modified the atmosphere within the channel. Since self-focusing depends upon the relative strengths of diffraction and nonlinear effects (Kerr lensing and plasma defocusing), the sudden reduction in the penetration rate shown in Figs. 3 and 6 corresponds to the point at which self-focusing significantly affects pointing stability (as indicated by the optical probe photos shown in Figs. 4, 5, and 7–11). The fact that femtosecond laser pulses penetrate more deeply in Fig. 5, when the incident laser intensity is 2.06×10^{14}W/cm^2, indicates that the weaker Kerr lens is more easily counteracted by diffraction and plasma defocusing than when $I_p = 3.08 \times 10^{14}$W/cm^2 (Fig. 4), while the observation that femtosecond laser pulses ($I_p = 3.08 \times 10^{14}$W/cm^2) penetrate more deeply into PbO silicate glass than into soda-lime silicate glass, as shown in Figs. 2 and 3, suggests that the Kerr lens is countered more effectively in PbO than in soda-lime silicate glass. Since the beam parameters were the same for the two glasses in Figs. 2(b) and 3, this behavior is independent of diffraction. Thus, it is likely that the increase in the penetration depth corresponds to an increase in the strength of plasma defocusing. Such an increase in the strength of plasma defocusing can be attributed to the presence of lead atoms trapped in the laser-machined channel after the impact of previous ablating laser pulses. The presence of lead atoms increases the amount of electrons available for, and lowers the threshold of, electron plasma generation.

VII. Femtosecond Laser Drilling at 1 kHz

As described in Section VI, the effects of self-focusing observed in Sections III and IV can be attributed to the presence of ablated material trapped inside the laser-machined channel. Therefore, these effects should be magnified if the laser repetition rate is increased, since there is less time for the ablated material to escape before the impact of subsequent laser pulses. To test this hypothesis, we conducted a set of femtosecond ablation experiments using a 1-kHz femtosecond laser system. This laser produced 150-fs laser pulses at 775 nm with 850 μJ/pulse. The focusing conditions were made to match the experiments described earlier. Thus, the maximum laser intensity that could be delivered to thetarget was $\sim 1.25 \times 10^{14}$ W/cm^2. Although this intensity was lower than the observed air-ionization threshold for laser pulses at 845 nm and 5 Hz, it was sufficient to induce air ionization at 775 nm and 1 kHz.

Due to the high average power on target ($\sim$850 mW) and the associated thermal load, attempts at hole drilling with long exposures (>10 s) at 1 kHz were unsuccessful. Therefore, a mechanical shutter was inserted into the experimental setup before the focal lens. During initial experiments, soda-lime and 45% PbO silicate glass samples were machined with 100 exposures with the shutter speed set at 1 s. A micrograph of the hole produced in PbO silicate glass is shown below in Fig. 12. This figure demonstrates evidence of self-focusing as indicated by the bristling of the tip of the hole.

In an attempt to decouple the thermal effects from the effects of self-focusing, holes were drilled into soda-lime silicate glass with the exposure period reduced to $1/125$ s, such that $\sim$8 laser pulses per exposure impacted the target surface. Therefore, the localized temperature of the target was not significantly changed during the experimental period. A micrograph of the hole produced in soda-lime silicate glass after 400 shutter exposures is

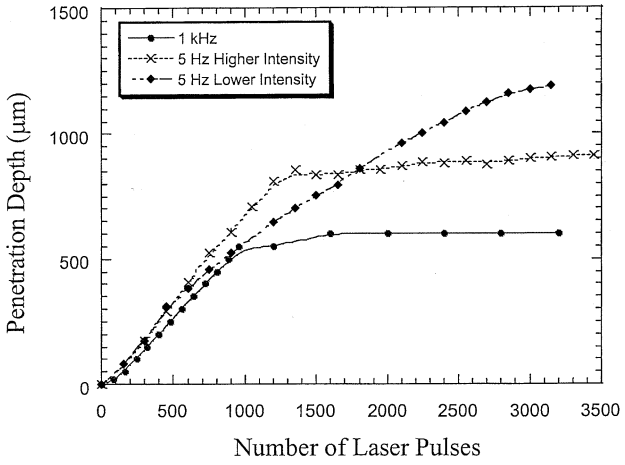

Fig. 14. Comparison the penetration depth in soda-lime silicate glass versus the number of laser pulses at 1 kHz and 5 Hz. For 1 kHz: $t_p = 150$ fs; $\lambda = 775$ nm; $E_p = 0.85$ mJ/pulse; $I_p = 1.25 \times 10^{14}$ W/cm^2. For 5 Hz higher intensity: $t_p = 110$ fs; $\lambda = 845$ nm; $E_p = 1.5$ mJ/pulse, $I_p = 3.08 \times 10^{14}$ W/cm^2 for 5 Hz Lower Intensity: $t_p = 110$ fs; $\lambda = 845$ nm; $E_p = 1.0$ mJ/pulse; $I_p = 2.06 \times 10^{14}$ W/cm^2.

shown below in Fig. 13. In order to compare the penetration rate at 1 kHz versus 5 Hz, the depth of this hole was measured periodically during drilling. The penetration rate versus the number of incident laser pulses at 1 kHz is plotted in Fig. 14, along with the data obtained from the optical probe experiments at 5 Hz shown in Fig. 6.

Fig. 14 shows that the initial penetration rate in the 1-kHz case is ~ 0.5 μm/pulse, similar to the low-repetition-rate experiments, despite significant differences in the experimental laser parameters. The 1-kHz data also exhibits a sudden rollover in the penetration rate which occurs at an earlier point than was observed at 5 Hz. The results of the latter experiments at intensities above the threshold for air ionization have been attributed to the interplay of nonlinear self-focusing phenomenon and the influence of residual ablated material within the laser-machined channel. These experiments at 1 kHz support this concept both in terms of increased beam steering (as shown in Figs. 12 and 13) and in the reduction in laser penetration rate (Fig. 14).

VIII. Summary

This study provides convincing evidence that residual ablated material remaining in the atmosphere of the channel during femtosecond-laser deep hole drilling affects the optical properties of the laser-machined channel. The presence of ablation residue can lead to nonlinear interactions between laser pulses and the atmosphere within the channel over a wide range of experimental conditions depending on the laser parameters: pulse duration, intensity, fluence, and repetition rate; and process parameters: atmospheric pressure, target material, and desired hole diameter. Furthermore, the results described in Section IV indicate that the processing mechanics can change during the course of hole drilling. Initially there are no adverse affects to drilling above the air ionization threshold; however after a critical depth there is a rollover in ablation and noticeable beam filamentation. This study demonstrates the interplay between hole drilling, beam propagation, and nonlinear beam interactions and helps to establish a link between self-focusing experiments [43], [47]–[53] and ablation rollover during femtosecond laser deep hole drilling [21], [54], [55].

Acknowledgment

The authors gratefully acknowledge the assistance of Dr. R. Negres, Dr. D. Hagan, and Dr. E. Van Stryland from the Nonlinear Optics Laboratory at The School of Optics/CREOL.

References

[1] B. C. Stuart, M. D. Feit, A. M. Rubenchik, B. W. Shore, and M. D. Perry, "Laser-induced damage in dielectrics with nanosecond to subpicosecond pulses," *Phys. Rev. Lett.*, vol. 74, pp. 2248–2251, 1995.

[2] S. Nolte, C. Momma, H. Jacobs, A. Tunnermann, B. N. Chichkov, B. Wellegehausen, and H. Welling, "Ablation of metals by ultrashort laser pulses," *J. Opt. Soc. Amer. B.*, vol. 14, pp. 2716–2722, 1997.

[3] X. Liu, D. Du, and G. Mourou, "Laser ablation and micromachining with ultrashort laser pulses," *IEEE J. Quantum Electron.*, vol. 33, pp. 1706–1716, 1997.

[4] N. Bloembergen, "Laser-induced electric breakdown in solids," *IEEE J. Quantum Electron.*, vol. QE-10, pp. 375–386, 1974.

[5] M. Bass and H. H. Barrett, "Laser-induced damage probability at 1.06 μm and 0.69 μm," *Appl. Opt.*, vol. 12, pp. 690–699, 1973.

[6] M. Bass and D. W. Fradin, "Surface and bulk laser-damage statistics and the identification of intrinsic breakdown processes," *IEEE J. Quantum Electron.*, vol. QE-9, pp. 890–896, 1973.

[7] P. P. Pronko, S. K. Dutta, J. Squier, J. V. Rudd, D. Du, and G. Mourou, "Machining of sub-micron holes using femtosecond laser at 800 nm," *Opt. Commun.*, vol. 114, pp. 106–110, 1995.

[8] S. Nolte, B. N. Chichkov, H. Welling, Y. Shani, K. Lieberman, and H. Terkel, "Nanostructuring with spatially localized femtosecond laser pulses," *Opt. Lett.*, vol. 24, pp. 914–916, 1999.

[9] F. Korte, S. Nolte, B. N. Chichkov, T. Bauer, G. Kamlage, T. Wagner, C. Fallnich, and H. Welling, "Far-field and near-field material processing with femtosecond laser pulses," *Appl. Phys. A.*, vol. 69 [Suppl.], pp. S7–S11, 1999.

[10] F. Korte, S. Adams, A. Egbert, C. Fallnich, A. Ostendorf, S. Nolte, M. Will, J.-P. Ruske, B. N. Chichkov, and A. Tunnermann, "Sub-diffraction limited structuring of solid targets with femtosecond laser pulses," *Opt. Express*, vol. 7, pp. 41–49, 2000.

[11] C. B. Schaffer, A. Brodeur, J. F. Garcia, and E. Mazur, "Micromachining bulk glass by use of femtosecond laser pulses with nanojoule energy," *Opt. Lett.*, vol. 26, pp. 93–95, 2001.

[12] K. Miura, J. Qiu, H. Inouye, T. Mitsuyu, and K. Hirao, "Photowritten optical waveguides in various glasses with ultrashort pulse laser," *Appl. Phys. Lett.*, vol. 71, pp. 3329–3331, 1997.

[13] K. Minoshima, A. M. Kowalevicz, I. Hartl, E. P. Ippen, and J. G. Fujimoto, "Photonic device fabrication in glass by use of nonlinear materials processing with a femtosecond laser oscillator," *Opt. Lett.*, vol. 26, pp. 1516–1518, 2001.

[14] J. Kruger and W. Kautek, "Femtosecond pulse visible laser processing of fiber composite materials," *Appl. Surf. Sci.*, vol. 106, pp. 383–389, 1996.

[15] J. Kruger and W. Kautek, "Femtosecond-pulse visible laser processing of transparent materials," *Appl. Surf. Sci.*, vol. 96–98, pp. 430–438, 1996.

[16] S. Baudach, J. Bonse, J. Kruger, and W. Kautek, "Ultrashort pulse laser ablation of polycarbonater and polymethylmethacrylate," *Appl. Surf. Sci.*, vol. 154–155, pp. 555–560, 2000.

[17] J. Sun, J. P. Longtin, and P. M. Norris, "Ultrafast laser micromachining of silica aerogels," *J. Non-Crystalline Solids*, vol. 281, pp. 39–47, 2001.

[18] M. D. Perry, B. C. Stuart, P. S. Banks, M. D. Feit, V. Yanovsky, and A. M. Rubenchik, "Ultrashort-pulse laser machining of dielectric materials," *J. Appl. Phys.*, vol. 85, pp. 6803–6810, 1999.

[19] A. A. Oraevsky, L. B. Da Silva, A. M. Rubenchik, M. D. Feit, M. E. Glinsky, M. D. Perry, B. M. Mammini, W. Small IV, and B. C. Stuart, "Plasma mediated ablation of biological tissues with nanosecond-to-femtosecond laser pulses: Relative role of linear and nonlinear absorption," *IEEE J. Select. Topics Quantum Electron.*, vol. 2, pp. 801–809, 1996.

[20] J. Neev, L. B. Da Silva, M. D. Feit, M. D. Perry, A. M. Rubenchik, and B. C. Stuart, "Ultrashort pulse lasers for hard tissue ablation," *IEEE J. Select. Topics Quantum Electron.*, vol. 2, pp. 790–800, 1996.

[21] L. Shah, J. Tawney, M. Richardson, and K. Richardson, "Femtosecond laser deep hole drilling of silicate glasses in air," *Appl. Surf. Sci.*, vol. 183, pp. 151–164, 2001.
[22] M. Bass and H. H. Barrett, "Avalanche breakdown and the probabilistic nature of laser-induced damage," *IEEE J. Quantum Electron.*, vol. QE-8, pp. 338–343, 1972.
[23] C.-H. Fan and J. P. Longtin, "Modeling optical breakdown in dielectrics during ultrafast laser processing," *Appl. Opt.*, vol. 40, pp. 3124–3131, 2001.
[24] J. P. Miotello and R. Kelly, "Critical assessment of thermal models for laser sputtering at high fluences," *Appl. Phys Lett.*, vol. 67, pp. 3535–3537, 1995.
[25] R. Kelly, A. Miotello, A. Mele, A. G. Giordani, J. W. Hastie, P. K. Scheneck, and H. Okabe, "Gas-dynamic effects in the laser-pulse sputtering of AIN: is there evidence for phase explosion," *Appl. Surf. Sci.*, vol. 133, pp. 251–269, 1998.
[26] H. W. K. Tom, G. D. Aumiller, and C. H. Brito-Cruz, "Time-resolved study of laser-induced disorder of Si surfaces," *Phys. Rev. Lett.*, vol. 60, pp. 1438–1441, 1988.
[27] P. Saeta, J.-K. Wang, Y. Siegal, N. Bloembergen, and E. Mazur, "Ultrafast electronic disordering during femtosecond laser melting of GaAs," *Phys. Rev. Lett.*, vol. 67, pp. 1023–1026, 1991.
[28] K. Sokolowski-Tinten and D. von der Linde, "Generation of dense electron-hole plasmas in silicon," *Phys. Rev. B.*, vol. 61, pp. 2643–2650, 2000.
[29] K. Sokolowski-Tinten, J. Bialkowski, A. Cavalleri, and D. von der Linde, "Transient states of matter during short pulse laser ablation," *Phys. Rev. B.*, vol. 81, pp. 224–227, 1998.
[30] ——, "Observation of a transient insulating phase of metals and semiconductors during short-pulse laser ablation," *Appl. Surf. Sci.*, vol. 127–129, pp. 755–760, 1998.
[31] A. Cavalleri, K. Sokolowski-Tinten, J. Bialkowski, and D. von der Linde, "Femtosecond laser ablation of gallium arsenide investigated with time-of-flight mass spectroscopy," *Appl. Phys. Lett.*, vol. 72, pp. 2385–2387, 1998.
[32] A. Cavalleri, K. Sokolowski-Tinten, J. Bialkowski, M. Schreiner, and D. von der Linde, "Femtosecond melting and ablation of semiconductors studied with time of flight mass spectroscopy," *J. Appl. Phys.*, vol. 85, pp. 3301–3309, 1999.
[33] D. Ashkenasi, A. Rosenfeld, H. Varel, M. Wahmer, and E. E. B. Campbell, "Laser processing of sapphire with picosecond and sub-picosecond pulses," *Appl. Surf. Sci.*, vol. 120, pp. 65–80, 1997.
[34] A. Rosenfeld, D. Ashkenasi, H. Varel, M. Wahmer, and E. E. B. Campbell, "Time resolved detection of particle removal from dielectrics on femtosecond laser ablation," *Appl. Surf. Sci.*, vol. 127–129, pp. 76–80, 1998.
[35] R. Stoian, H. Varel, A. Rosenfeld, D. Ashkenasi, R. Kelly, and E. E. B. Campbell, "Ion time-of-flight analysis of ultrashort pulsed laser-induced processing of Al_2O_3," *Appl. Surf. Sci.*, vol. 165, pp. 44–55, 2000.
[36] *Optical Glass Catalog*, 18 642.
[37] R. W. Boyd, *Nonlinear Optics*. New York: Academic, 1992, pp. 159–178. and 241-264.
[38] A. Chiron, G. Bonnaud, A. Dulieu, J. L. Miquel, G. Malka, M. Louis-Jacquet, and G. Mainfray, "Experimental observations and simulations on relativistic self-guiding of an ultra-intense laser pulse in underdense plasmas," *Phys. Plasma*, vol. 3, pp. 1373–1401, 1996.
[39] W. C. Rado, "The nonlinear third order dielectric susceptibility coefficients of gasses and optical third harmonic generation," *Appl. Phys. Lett.*, vol. 4, pp. 123–125, 1967.
[40] D. V. Vlasov, R. A. Garaev, V. V. Korobkin, and R. V. Servo, "Measurement of nonlinear polarizability of air," *Sov. Phys. JETP*, vol. 49, pp. 1033–1036, 1979.
[41] Y. Shimoji, A. T. Fay, R. S. F. Chang, and N. Djeu, "Direct measurement of the nonlinear refractive index of air," *J. Opt. Soc. Amer. B.*, vol. 6, pp. 1994–1998, 1989.
[42] W. E. Martin and R. J. Winfield, "Nonlinear effects on pulsed laser propagation in the atmosphere," *Appl. Opt.*, vol. 27, pp. 567–577, 1988.
[43] A. Braun, G. Korn, X. Liu, D. Du, J. Squier, and G. Mourou, "Self-channeling of high-peak-power femtosecond laser pulses in air," *Opt. Lett.*, vol. 20, pp. 73–75, 1995.
[44] C. E. Max, J. Arons, and A. B. Langdon, "Self-modulation and self-focusing of electromagnetic waves in plasmas," *Phys. Rev. Lett.*, vol. 33, pp. 209–212, 1974.
[45] J. Jackson, *Classical Electrodynamics*, 2nd ed. New York: Wiley, 1975, p. 238.
[46] R. Fedosejevs, X. F. Wang, and G. D. Tsarkiris, "Onset of relativistic self-focusing in high density gas jet targets," *Phys. Rev. E.*, vol. 56, pp. 4615–4639, 1997.
[47] M. Mlejnek, M. Kolesik, J. V. Moloney, and E. M. Wright, "Optically turbulent femtosecond light guided in air," *Phys. Rev. Lett.*, vol. 83, pp. 2938–2941, 1999.
[48] S. Tzortakis, M. A. Franco, Y.-B. Andre, A. Chiron, B. Lamouroux, B. S. Prade, and A. Mysyrowicz, "Formation of a conducting channel in air by self-guided femtosecond laser pulses," *Phys. Rev. E.*, vol. 60, pp. R3505–RS3507, 1999.
[49] S. Tzortakis, L. Berge, A. Couairon, M. Franco, B. Prade, and A. Mysyrowicz, "Breakup and fusion of self-guided femtosecond light pulses in air," *Phys. Rev. Lett.*, vol. 86, pp. 5470–5473, 2001.
[50] K. Yamada, W. Watanabe, T. Toma, and K. Itoh, "In *situ* observation of photoinduced refractive-index changes in filaments formed in glasses by femtosecond laser pulses," *Opt. Lett.*, vol. 26, pp. 19–21, 2001.
[51] S. Tzortzakis, L. Sudrie, M. Franco, B. Prade, A. Mysyrowicz, A. Couairon, and L. Berge, "Self-guided propagation of ultrashort IR laser pulses in fused silica," *Phys. Rev. Lett.*, vol. 87, no. 1–4, p. 213 902, 2001.
[52] L. Sudrie, A. Couairon, M. Franco, B. Lamouroux, B. Prade, S. Tzortzakis, and A. Mysyroawicz, "Femtosecond laser-induced damage and filamentary propagation in fused silica," *Phys Rev. Lett.*, vol. 89, no. 1-4, p. 186 601, 2002.
[53] S.-H. Cho, H. Kumagai, and K. Midorikawa, "In situ observation of dynamics of plasma formation and refractive index modification in silica glasses excited by a femtosecond laser," in *Proc. 3rd Int. Symp. Laser Precision Microfabrication*, vol. 4830, Osaka, Japan, 2003, pp. 557–566.
[54] S. M. Klimentov, T. V. Kononenko, P. A. Pivovarov, S. V. Garnov, V. I. Konov, D. Breitling, and F. Dausinger, "Role of gas environment in the process of deep hole drilling by ultra-short laser pulses," in *Proc. 3rd Int. Symp. Laser Precision Microfabrication*, vol. 4830, Osaka, Japan, 2003, pp. 515–520.
[55] D. Ashkenasi, G. Herbst, A. Rosenfeld, H. Varel, M. Lorenz, R. Stoian, and E. E. B. Campbell, "Laser ablation and structuring of transparent materials with ultrashort laser pulses," *Proc. High Power Laser Ablation*, vol. 3343, pp. 400–410, 1998.
[56] O. G. Kosareva, V. P. Kandidov, A. Brodeur, C. Y. Chien, and S. L. Chin, "Conical emission from laser plasma interactions in the filamentation of powerful ultrashort laser pulses in air," *Opt. Lett.*, vol. 22, pp. 1332–1334, 1997.

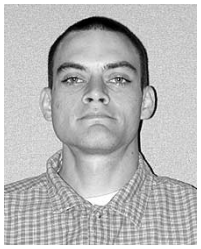

Lawrence Shah received the Ph.D. degree in optical physics from the University of Central Florida, Orlando, in 2001.

From 1997 to 2001, he conducted research for the Laser Plasma Laboratory at the University of Central Florida. From 2001 to 2002, he worked as a Post-Doctoral Researcher with the Short Pulse Laser Applications and Technology group of the Laser Science and Technology division at Lawrence Livermore National Laboratory. In 2002, he joined the Application Research Laboratory of IMRA America, Inc., Ann Arbor, MI. His research interests include femtosecond laser design, ultrafast laser–material interaction, and laser materials processing.

Jess Tawney received the B.S. and M.S. degrees in electrical engineering from the University of Central Florida, Orlando, in 1999 and 2000, respectively.

In 1999, he worked at the Laser Plasma Laboratory as a Junior Engineer to assist graduate students. He was accepted in the graduate electrical engineering program in 1999 where he chose the electro optics emphasis and subsequently received a fellowship at the School of Optics/CREOL. He returned to the Laser Plasma Laboratory as a Research Assistant where he worked on improving the contrast of ultrahigh-power chirped pulse amplified lasers. In 2000, he joined the Electro Optics group at the Charles Stark Draper Laboratory, Cambridge, MA.

Martin Richardson graduated from Imperial College and London University. He currently directs the Laser Plasma and Laser Development Laboratories, University of Central Florida (UCF), Orlando, which has research programs on the development of new high-power solid-state lasers, laser-plasma EUV sources for lithography, high-resolution biological X-ray microscopy, and the interaction of high-intensity femtosecond laser light with matter. He is also part of the Richardson Group, a multiinstitutional research team studying laser micro-processing of materials, including biological materials, with femtosecond lasers. His career has been in the fields of high-power laser development, laser interaction with matter, dense plasma physics, X-ray science, and low-energy nuclear physics. His previous primary positions were at the University of Rochester's LLE laser fusion program and the Institute of Optics, and, prior to that, the NRC Hertzberg Laboratory in Canada. He has also held visiting positions at other major laser institutions, including the Max Born Institute, Berlin, Germany, the Institute for Laser Engineering, Osaka, Japan, the Max Planck Institute for Quantum Optics, Munich, Germany, the Lebedev Institute, Moscow, Russia, and institutions in Australia, Canada, and the U.S. He has published over 300 scientific articles in professional scientific journals and holds nine patents (most licensed), with several others pending.

Dr. Richardson has chaired many international conferences including IQEC, ICHSP, and several SPIE meetings. He is a former Associate Editor of the IEEE JOURNAL OF QUANTUM ELECTRONICS, a recipient of the Schardin Medal and several awards at UCF, and a Fellow of the Optical Society of America.

Kathleen Richardson is an Associate Professor of Optics, Chemistry and Mechanical, Materials and Aerospace Engineering at the School of Optics, University of Central Florida (UCF), Orlando. She has just returned to UCF following a leave of absence at SCHOTT North America, Regional R&D, Duryea, PA, where she served as Manager of their Materials Development and Technologies groups since January 2002. She joined UCF in 1992 following several years at the University of Rochester's Laboratory for Laser Energetics where she conducted research on ion-exchange strengthened laser glass, passive and active liquid crystal-based optics and sol gel-derived materials. Her UCF research programs examine the role of structure/property relationships in a range of glass and ceramic media used in optical applications. In addition to supervising research programs in infrared glasses for use in integrated optics applications, her group also has industrial and government supported research programs evaluating consumables used in the chemo-mechanical polishing (CMP) of semiconductor materials and in the assessment of diffusion and crystallization behavior of bulk photosensitive glasses. She has authored more than 75 refereed publications, proceedings, and book chapters.

Dr. Richardson is a Fellow of the Society of Glass Technology.